IEEE Access
Multidisciplinary | Rapid Review | Open Access Journal

SPECIAL SECTION ON CYBER-PHYSICAL-SOCIAL COMPUTING AND NETWORKING

Received April 8, 2018, accepted May 4, 2018, date of publication May 22, 2018, date of current version August 28, 2018.

Digital Object Identifier 10.1109/ACCESS.2018.2838123

A BP Neural Network-Based Communication Blind Signal Detection Method With Cyber-Physical-Social Systems

XIN LIU[1], YANJU ZHOU[1], ZONGRUN WANG[1], AND XIAOHONG CHEN[1,2]

[1]School of Business, Central South University, Changsha 410083, China
[2]Principal's Office, Hunan University of Commerce, Changsha 410205, China

Corresponding author: Yanju Zhou (zyj4258@sina.com)

This work was supported in part by the National Natural Science Foundation of China under Grants 71471178, 71371194, and 71171201, in part by the State Key Program of National Natural Science Foundation of China under Grant 71431006 and Grant71631008, in part by the Projects of International Cooperation and Exchanges NSFC under Grant 71210003, in part by the Major Project for National Natural Science Foundation of China under Grant 71790615, in part by the Fundamental Research Funds for the Central Universities under Grant 2011RWSK003, and in part by the Program for New Century Excellent Talents in University under Grant NCET-13-0604.

ABSTRACT The development of wireless communication technologies will lead to an increase of rapid-time-variants featured occasions and physical occasions of small-data-size communication in network, and the modulation system diversification resulting from social group densification. Though traditional blind signal detection approaches have been improved by reducing their excessive reliance on data size, they still have the defects of various postulated conditions in new settings, complicated computation, unstable detection effect and high error rate. This paper aims to explore a communication blind signal detection method in the setting of cyber-physical-social systems in the field of back-propagation (BP) neural network. First, a BP neural network is used as the equalizer, an error function is redefined, and the back-propagation algorithm is used to train and adjust blind signal data deviation and to update network weight rules for adaptation to network settings with rapid time-variants. Second, a double-sigmoid BP neural network excitation function is constructed to improve poor multiple information processing and network performances resulting from social group densification. Third, self-adaptive variable step size for physical devices' power is constructed to adjust the conflict between convergence rate and steady-state error caused by different powers with the increase of small-data-size communication. Finally, an output vector is made to be closest to an expected vector; thereby, blind signal detection rate of social groups' communication using physical devices in the cyber environment can be improved. The experiments show that the communication blind signal detection method proposed in the paper improves signal detection precision, and reduces omission rate (below 2%). Besides, the method is characterized by minor error, removes deficiencies of traditional methods for blind signal extraction, and can effectively accomplish blind signal detection.

INDEX TERMS BP neural network, activation function, blind signal detection, cyber-physical-social systems.

I. INTRODUCTION

In the field of network information technologies, a cyber system is composed of nodes and lines representing various objects and their interrelations. In mathematics, a cyber system is a map, generally a weighted graph; and it also has a physical connotation–a model abstracted from a specific type of practical problems. Physical device is a generic term for different tools in network (incl. node devices, communication devices, terminal devices, storage devices, power systems, etc.) and other hardware devices for their service. A social group is a form of social organization integrated by specific relations for common activities, a network with mutual relations, and one of the basic units constituting a society. With the progress of science and technologies as well as a rapid development of wireless communication technologies, it is in urgent need to develop a modern and high-efficiency communication network used by all social groups in the world, and higher standards are raised for real-time performance and precision of network communication. In the communication process of social groups using network,

the communication system receives and detects blind signals as communication data. Without any prior knowledge other than source signals and transmission channels, blind detection of communication signals is a process in which the existence and regularity of signals are identified and judged merely based on the received signals. Therefore, researches on blind detection of communication signals are of vital practical significance.

Urkowitz H firstly presented a blind signal detection algorithm [1], and published a paper about signal detection. In different scientific fields, especially those associated with signals (such as voice signal separation and identification, wireless communication system, and processing of biological signals), blind signal detection algorithms have been substantially and thoroughly studied. In recent years, researchers both in China and abroad have extensively and systematically studied signal detection algorithms, including the delay multiplication detection method [2], power spectrum reprocessing method [3], period spectrum method [4], etc. However, most of the signal detection methods requires priori information (such as spreading code parameters and carrier frequency of received signal), and are not blind detection (called codeless detection in some literatures) in the strict sense. For blind signal detection, main detection methods in researches include energy method [5], least square method [6], square method [7], etc. So far, various practical application problems remain to be solved, including poor disturbance resistance, inaccuracy of detection data, etc. Blind signal in network communication is a non-stationary random signal, while traditional detection algorithm cannot effectively extract impulse response features of signals and show relatively low detection accuracy.

For blind signal processing, $y(n) = Ax(n)$, it is assumed that an unknown signal source utilizing sensor linear aliasing method releases detection signal, and $R^{m\times n}$ is an unknown hybrid matrix. $s(t) \in R^n$ is a n-dimension blind signal; $y(t) \in R^m$ is a detected signal; A is an equalizer. Based on traditional methods, composite signals cannot be completely separated, since there is little known information about blind signals. Blind signal processing has been repeatedly reported in many literatures. Methods in literatures [7] and [8] are based on assumed conditions for blind signal detection, and are inconsistent with actual conditions; though algorithms in literatures [9]–[11] can be used to detect blind signal in a voice communication system in a relatively precise way, the complicated operation procedures make them less applicable for actual practice. With the methods presented in literatures [12], [13], the final detection results show low accuracy, and fail to realize the purpose of effectively detecting blind signal. Therefore, to avoid the deficiencies (high operation complexity, inaccurate detection result, etc.) of traditional methods, the paper proposes a BP neural network-based blind signal detection method with cyber-physical-social systems. Cyber, physical, and social systems are fused to systematically and comprehensively detect blind signal in communication, and simulation experiments are conducted to verify the effectiveness and accurateness of this method in identifying and detecting blind signal.

Specially, the main contributions of the BPNNCBSD-CPSS scheme include the following:

(1). Under network environment, blind signals generated by intelligent communication devices used by social groups are tasked as data sample and input the cyber-physical-social systems-integrated BP neural network model; back-propagation algorithm is used to train and adjust data deviation and network weight of blind signal and to make output vectors possibly much closer to expected vectors. As cyber, physical and social systems are fused, problems of a pure BP neural network algorithm, including a high possibility of local minimum and slow algorithm convergence, are solved.

(2). Experiments are conducted to verify the proposed blind signal detection method, which improves the signal detection precision, reduces the omission rate, and can effectively complete achieve blind signal detection. The detection method is characterized by a high precision (reaching 91%), a small error rate (below 0.1) and a low omission rate (below 2%).

The remainder of the paper is organized as follows. In Section II, we described relevant work, constructing a cyber-physical-social systems-fused BP neural network model, and utilized the model for detection of blind signal. In Section III, we conducted several experiments, analyzed the four groups of experiments, and obtained experimental results shown in figures. Finally, we draw a conclusion, summarize the paper, and present the orientation for future work in Section IV.

II. A BP NEURAL NETWORK-BASED COMMUNICATION BLIND SIGNAL DETECTION MODEL WITH CYBER-PHYSICAL-SOCIAL SYSTEMS

A. PRINCIPLE OF BP NEURAL NETWORK-BASED COMMUNICATION BLIND SIGNAL DETECTION

Connecting multiple neurons to each other can construct an artificial neural network, which effectively processes signals and outputs signal units after connecting different neural units assigned with different weights [14]–[17]; in different artificial neural networks, a back-propagation network (abbr. BP network) is the neural network model most frequently used. BP network is a feed-forward hierarchical network, which is formed by full connection of three hierarchical structures, an input layer, an output layer, and a hidden layer. Motivation-model unit outputs of every originating node in an input layer make up input signals of the second layer of neurons, while the motivation-model unit outputs of nodes in a second layer make up the input models of a third layer; the same way applies to other layers. Every neuron layer only contains output signals of the former layer as its inputs. Output signals of output layer neurons are full response to motivation models generated by originating nodes of an input layer [18]–[21].

A BP neural network structure applying for communication blind signal detection is described below. Meanwhile, to facilitate explanation, network sending signals are written in plural form.

$$x(n-i) = x^R(n-i) + ix^I(n-i) \tag{1}$$

It is assumed that an input layer inputs n signals, namely n neurons. The amount of neurons in a hidden layer is q1; the excitation function is φ_1, the input is $s_{q1}(n)$, and the output is $b_{q1}(n)$. An output layer has q2 neurons; the excitation function is φ_2, and the input and output are $c_{q2}(n)$ and $y_{q2}(n)$ respectively. The connection weight between the input layer and the hidden layer is $w_{mi}(n)$, while that between the hidden layer and the output layer is $v_{ij}(n)$; and the expected output is $\tilde{y}_{q2}(n)$.

The weight from the input layer to the hidden layer is expressed as

$$w_{mi}(n) = w^R_{mi}(n) + j \cdot w^I_{mi}(n) \tag{2}$$

The weight from the hidden layer to the output layer is expressed as

$$v_{ij}(n) = v^R_{ij}(n) + j \cdot v^I_{ij}(n) \tag{3}$$

According to the forward propagation of input signals, the formulas are as below.

The input vector of the hidden layer neurons is

$$s_{q1}(n) = \sum_i w_{mi} x(n-i) \tag{4}$$

The output vector of the hidden layer neurons is

$$b_{q1}(n) = \varphi_1(s_{q1}(n)) = \varphi_1(s^R_{q1}(n)) + j \cdot \varphi_1(s^I_{q1}(n)) \tag{5}$$

The input vector of the output layer neurons is

$$c_{q2}(n) = \sum v_{ij}(n) b_{q1}(n) \tag{6}$$

The output vector of the output layer neurons is

$$y_{q2}(n) = \varphi_2(c_{q2}(n)) \tag{7}$$

According to the traditional CMA algorithm, the error function is defined as

$$J(n) = \frac{1}{2}\left[|y(n)|^2 - R^2\right]^2, \quad \text{where } R^2 = \frac{E\left[|\tilde{a}(n)|^4\right]}{E\left[|\tilde{a}(n)|^2\right]} \tag{8}$$

With the steepest gradient descent method, weights are adjusted layer by layer according to network back transmission of signals. Based on the signal transmission manner, the iterative formulas adjusting connection weight of every layer are

$$\begin{cases} w(n+1) = w(n) - \eta_1 \dfrac{\partial J(n)}{\partial w(n)} \\ v(n+1) = v(n) - \eta_2 \dfrac{\partial J(n)}{\partial v(n)} \end{cases} \tag{9}$$

where η_1 and η_2 are iterative step sizes of the network connection weights.

$$\begin{cases} \dfrac{\partial J(n)}{\partial w(n)} = 2 \cdot [|y_{q2}(n)|^2 - R^2] \cdot |y_{q2}(n)| \\ \qquad \cdot [\dfrac{\partial |y_{q2}(n)|}{\partial w^R(n)} + j\dfrac{\partial |y_{q2}(n)|}{\partial w^I(n)}] \\ \dfrac{\partial J(n)}{\partial v(n)} = 2 \cdot [|y_{q2}(n)|^2 - R^2] \\ \qquad \cdot |y_{q2}(n)| \cdot [\dfrac{\partial |y_{q2}(n)|}{\partial v^R(n)} + j\dfrac{\partial |y_{q2}(n)|}{\partial v^I(n)}] \end{cases} \tag{10}$$

Based on the above formulas, it can be found that a BP neural network applies to both real number and complex number categories, while the main application difference for the two is to distinguish real parts and imaginary parts when processing data. The final results are usually satisfactory [22].

As sent sequences are plural, and the variation of the excitation function for the whole system shall fall in the scope of complex number correspondingly. The following part introduces connection weight iteration of a hidden layer of a BP neural network within the scope of complex number.

(1). The iteration of connection weight from an input layer to a hidden layer is

$$\frac{\partial J(n)}{\partial w(n)} = 2 \cdot [|y_{q2}(n)|^2 - R^2] \cdot |y_{q2}(n)| \cdot [\frac{\partial |y_{q2}(n)|}{\partial w(n)}] \tag{11}$$

It can be known from the above formulas that, to obtain $\frac{\partial J(n)}{\partial w_{mi}(n)}$, only the solution of $\frac{\partial |y_{q2}(n)|}{\partial w_{mi}(n)}$ is required. Since the weight falls in the scope of complex number, both real parts and imaginary parts shall be iterated when iterating connection weights. Gathering up the threads, we can obtain the following formulas

$$\frac{\partial |y_{q2}(n)|}{\partial w_{mi}(n)} = \frac{\partial |y_{q2}(n)|}{\partial w^R_{mi}(n)} + j\frac{\partial |y_{q2}(n)|}{\partial w^I_{mi}(n)} \tag{12}$$

$$|y_{q2}(n)| = \sqrt{y_{q2}(n) y^*_{q2}(n)} \tag{13}$$

where $y^*_{q2}(n)$ is the conjugate of $y_{q2}(n)$.

Then, we can obtain

$$\begin{cases} \dfrac{\partial |y_{q2}(n)|}{\partial w^R_{mi}(n)} = \dfrac{\partial \sqrt{y_{q2}(n) y^*_{q2}(n)}}{\partial w^R_{mi}(n)} = \dfrac{1}{2|y_{q2}(n)|} \dfrac{\partial [y_{q2}(n) y^*_{q2}(n)]}{\partial w^R_{mi}(n)} \\ \dfrac{\partial |y_{q2}(n)|}{\partial w^I_{mi}(n)} = \dfrac{\partial \sqrt{y_{q2}(n) y^*_{q2}(n)}}{\partial w^I_{mi}(n)} = \dfrac{1}{2|y_{q2}(n)|} \dfrac{\partial [y_{q2}(n) y^*_{q2}(n)]}{\partial w^I_{mi}(n)} \end{cases} \tag{14}$$

(2). The iteration formula for the connection weight from a hidden layer to an output layer is as below.

The method to solve the connection weight from an input layer to a hidden layer is same as above.

$$\begin{aligned} \frac{\partial J(n)}{\partial v(n)} &= 2 \cdot [|y_{q2}(n)|^2 - R^2] \cdot |y_{q2}(n)| \cdot [\frac{\partial |y_{q2}(n)|}{\partial v(n)}] \\ \frac{\partial |y_{q2}(n)|}{\partial v_{ij}(n)} &= \frac{\partial |y_{q2}(n)|}{\partial v^R_{ij}(n)} + j\frac{\partial |y_{q2}(n)|}{\partial v^I_{ij}(n)} \end{aligned} \tag{15}$$

Then, we can obtain

$$\begin{cases} \dfrac{\partial\left|y_{q2}(n)\right|}{\partial v_{ij}^{R}(n)}=\dfrac{\partial\sqrt{y_{q2}(n)y_{q2}^{*}(n)}}{\partial v_{ij}^{R}(n)}=\dfrac{1}{2\left|y_{q2}(n)\right|}\dfrac{\partial[y_{q2}(n)y_{q2}^{*}(n)]}{\partial v_{ij}^{R}(n)} \\ \dfrac{\partial\left|y_{q2}(n)\right|}{\partial v_{ij}^{I}(n)}=\dfrac{\partial\sqrt{y_{q2}(n)y_{q2}^{*}(n)}}{\partial v_{ij}^{I}(n)}=\dfrac{1}{2\left|y_{q2}(n)\right|}\dfrac{\partial[y_{q2}(n)y_{q2}^{*}(n)]}{\partial v_{ij}^{I}(n)} \end{cases} \tag{16}$$

B. "CYBER-PHYSICAL-SOCIAL SYSTEMS" COMBINED BP NEURAL NETWORK DETECTION MODEL OF BLIND COMMUNICATION SIGNAL

The communication blind signal detection model with cyber-physical-social systems adopts a three-layer BP neural system, which is constructed by an input layer, a hidden layer, and an output layer. When seeking for input signals, the BP neural network can be taken as an equalizer; the power of the physical entity is used to determine weight, while the excitation function is determined according to the density of social groups [23]–[25]. The sketch of a 3-layer BP network is shown in Fig. 1.

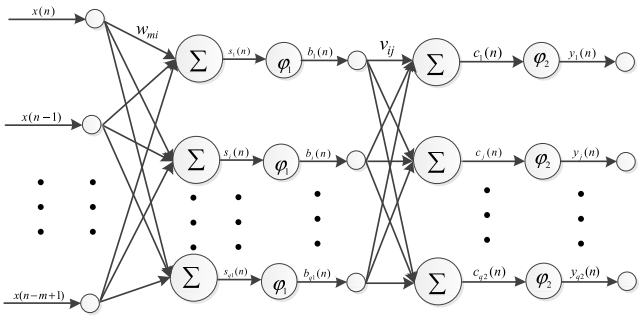

FIGURE 1. Structure drawing of a 3-layer BP neural network with cyber-physical-social systems.

The input layer is assumed to input n signals (n neurons), which are expressed as $m = 1, 2, \ldots, n$. The hidden layer has q_1 neurons, which were expressed as $i = 1, 2, \ldots, q_1$; the excitation function is φ_1, the input is $s_{q1}(n)$, and the output result after excitation is $b_{q1}(n)$. The output layer has q_2 neurons; the excitation function is φ_2, every neuron is expressed as $j = 1, 2, \ldots, q_2$, the input of the output layer is $c_{q2}(n)$, and the output of the output layer is $y_{q2}(n)$. The connection weights between the input layer and the hidden layer and between the hidden layer and the output layer are $w_{mi}(n)$ and $v_{ij}(n)$ respectively, while the expected output is $\tilde{y}_{q2}(n)$.

1) BP NEURAL NETWORK-BASED ERROR FUNCTION

Based on the traditional constant modulus algorithm (CMA) and BP algorithm, a new network error function is redefined.

$$J(n)=\frac{1}{2}\left[\ln(|y(n)|^{2}\Big/R^{2})\right]^{2} \tag{17}$$

A BP neural network and CMA share a same definition for R^2 of communication blind signal.

$$R^{2}=\frac{E\left[|y(n)|^{4}\right]}{E\left[|y(n)|^{2}\right]} \tag{18}$$

2) BP NEURAL NETWORK-BASED WEIGHT UPDATE RULES

The formula for the serial forward transmission of input signal under QPSK system is as follow.

The formula for input signal is

$$x(n-m+1)=x_{R}(n-m+1)+jx_{I}(n-m+1) \tag{19}$$

Formulas for weights of the BP neural network-based layers are

$$\begin{cases} w_{mi}(n)=w_{mi,R}(n)+jw_{mi,I}(n) \\ v_{ij}(n)=v_{ij,R}(n)+jv_{ij,I}(n) \end{cases} \tag{20}$$

The input vector of the hidden layer neurons is

$$\begin{aligned} &s_{q1}(n) \\ &=\sum_{m=1}^{p}w_{mi}(n)\cdot x(n-m+1) \\ &=\sum_{m=1}^{p}\left[w_{mi}^{R}(n)x_{R}(n-m+1)-w_{mi}^{I}(n)x_{I}(n-m+1)\right] \\ &\quad+j\sum_{m=1}^{p}\left[w_{mi}^{R}(n)x_{I}(n-m+1)+w_{mi}^{I}(n)x_{R}(n-m+1)\right] \end{aligned} \tag{21}$$

The output vector of the hidden layer neurons is

$$\begin{aligned} b_{q1}(n)&=\varphi_{1}(s_{q1}(n))=\varphi_{1}(s_{q1}^{R}(n))+j\varphi_{1}(s_{q1}^{I}(n)) \\ &=\varphi_{1}\left\{\sum_{m=1}^{p}\left[w_{mi}^{R}(n)x_{R}(n-m+1)-w_{mi}^{I}(n)\right.\right. \\ &\qquad\left.\left.\times x_{I}(n-m+1)\right]\right\} \\ &\quad+j\varphi_{1}\left\{\sum_{m=1}^{p}\left[w_{mi}^{R}(n)x_{I}(n-m+1)+w_{mi}^{I}(n)\right.\right. \\ &\qquad\left.\left.\times x_{R}(n-m+1)\right]\right\} \end{aligned} \tag{22}$$

The input vector of the output layer neurons is

$$\begin{aligned} c_{q2}(n)&=\sum_{i=1}^{q1}v_{ij}(n)b_{q1}(n)=\sum_{i=1}^{q1}[v_{ij}^{R}(n)b_{q1}^{R}(n)-v_{ij}^{I}(n)b_{q1}^{I}(n)] \\ &\quad+j\cdot\sum_{i=1}^{q1}[v_{ij}^{R}(n)b_{q1}^{I}(n)+v_{ij}^{I}(n)b_{q1}^{\mathrm{R}}(n)] \end{aligned} \tag{23}$$

The output vector of the output layer neurons is

$$y_{q2}(n)=\varphi_{2}(c_{q2}(n))=\varphi_{2}(c_{q2}^{R}(n))+j\varphi_{2}(c_{q2}^{I}(n)) \tag{24}$$

Similarly, with the steepest gradient descent method, weights are adjusted layer by layer according to network back transmission. The formulas are

$$\begin{cases} w(n+1) = w(n) - \eta_1 \dfrac{\partial J(n)}{\partial w(n)} \\ v(n+1) = v(n) - \eta_2 \dfrac{\partial J(n)}{\partial v(n)} \end{cases} \tag{25}$$

where η_1 and η_2 are iterative step sizes of the network connection weights.

$$\begin{aligned} \frac{\partial J(n)}{\partial w(n)} &= 2 \cdot \left[\ln\left(|y_{q2}(n)|^2 \Big/ R^2\right)\right] \cdot |y_{q2}(n)| \\ &\quad \cdot \left[\frac{\partial |y_{q2}(n)|}{\partial w^R(n)} + j\frac{\partial |y_{q2}(n)|}{\partial w^I(n)}\right] \\ \frac{\partial J(n)}{\partial v(n)} &= 2 \cdot \left[\ln\left(|y_{q2}(n)|^2 \Big/ R^2\right)\right] \cdot |y_{q2}(n)| \\ &\quad \cdot \left[\frac{\partial |y_{q2}(n)|}{\partial v^R(n)} + j\frac{\partial |y_{q2}(n)|}{\partial v^I(n)}\right] \end{aligned}$$

(1). Iteration of the Connection Weight from the Input Layer to the Hidden Layer

$$\frac{\partial J(n)}{\partial w_{mi}(n)} = 2 \cdot \left[\ln\left(|y_{q2}(n)|^2 \Big/ R^2\right)\right] \cdot |y_{q2}(n)| \cdot \left[\frac{\partial |y_{q2}(n)|}{\partial w_{mi}(n)}\right]$$

It can be known from the above formulas that, to obtain $\frac{\partial J(n)}{\partial w_{mi}(n)}$, only the solution of $\frac{\partial |y_{q2}(n)|}{\partial w_{mi}(n)}$ is required.

Since the weight falls in the scope of complex number, both real parts and imaginary parts shall be iterated when iterating connection weights. Gathering up the threads, we can obtain the following formulas

$$\frac{\partial |y_{q2}(n)|}{\partial w_{mi}(n)} = \frac{\partial |y_{q2}(n)|}{\partial w^R_{mi}(n)} + j\frac{\partial |y_{q2}(n)|}{\partial w^I_{mi}(n)} \tag{26}$$

$$|y_{q2}(n)| = \sqrt{y_{q2}(n) y^*_{q2}(n)} \tag{27}$$

In the formulas, $y^*_{q2}(n)$ is the conjugate of $y_{q2}(n)$.

Then, we can obtain

$$\begin{aligned} \frac{\partial |y_{q2}(n)|}{\partial w^R_{mi}(n)} &= \frac{\partial \sqrt{y_{q2}(n) y^*_{q2}(n)}}{\partial w^R_{mi}(n)} \\ &= \frac{1}{2|y_{q2}(n)|} \frac{\partial [y_{q2}(n) y^*_{q2}(n)]}{\partial w^R_{mi}(n)} \\ &= \frac{1}{|y_{q2}(n)|} \cdot [\varphi(c^R_{q2}(n))\varphi'(c^R_{q2}(n)) \frac{\partial c^R_{q2}(n)}{\partial w^R_{mi}(n)} \\ &\quad + \varphi(c^I_{q2}(n))\varphi'(c^I_{q2}(n)) \frac{\partial c^I_{q2}(n)}{\partial w^R_{mi}(n)} \frac{\partial |y_{q2}(n)|}{\partial w^I_{mi}(n)} \\ &= \frac{1}{|y_{q2}(n)|} \cdot [\varphi(c^R_{q2}(n))\varphi'(c^R_{q2}(n)) \frac{\partial c^R_{q2}(n)}{\partial w^I_{mi}(n)} \\ &\quad + \varphi(c^I_{q2}(n))\varphi'(c^I_{q2}(n)) \frac{\partial c^I_{q2}(n)}{\partial w^I_{mi}(n)} \end{aligned} \tag{28}$$

In the formulas,

$$\begin{aligned} \frac{\partial c^R_{q2}(n)}{\partial w^R_{mi}(n)} &= \frac{\partial [v^R_{ij}(n) b^R_{q1}(n) - v^I_{ij}(n) b^I_{q1}(n)]}{\partial w^R_{mi}(n)} = v^R_{ij}(n)\varphi'(s^R_{q1}(n)) \\ &\quad \times \frac{\partial s^R_{q1}(n)}{\partial w^R_{mi}(n)} - v^I_{ij}(n)\varphi'(s^I_{q1}(n)) \frac{\partial s^I_{q1}(n)}{\partial w^R_{mi}(n)} \\ &= v^R_{ij}(n)\varphi'(s^R_{q1}(n)) x^R(n-m+1) - v^I_{ij}(n)\varphi' \\ &\quad \times (s^I_{q1}(n)) x^I(n-m+1) \end{aligned} \tag{29}$$

In a similar way, we can obtain

$$\begin{aligned} \frac{\partial c^I_{q2}(n)}{\partial w^R_{mi}(n)} &= v^R_{ij}(n)\varphi'(c^I_{q2}(n)) x^I(n-m+1) \\ &\quad - v^I_{ij}(n)\varphi'(c^R_{q2}(n)) x^R(n-m+1) \end{aligned} \tag{30}$$

$$\begin{aligned} \frac{\partial c^R_{q2}(n)}{\partial w^I_{mi}(n)} &= -v^R_{ij}(n)\varphi'(c^R_{q2}(n)) x^I(n-m+1) \\ &\quad - v^I_{ij}(n)\varphi'(c^I_{q2}(n)) x^R(n-m+1) \end{aligned} \tag{31}$$

$$\begin{aligned} \frac{\partial c^I_{q2}(n)}{\partial w^I_{mi}(n)} &= v^R_{ij}(n)\varphi'(s^I_{q1}(n)) x^R(n-m+1) \\ &\quad - v^I_{ij}(n)\varphi'(s^R_{q1}(n)) x^I(n-m+1) \end{aligned} \tag{32}$$

Based on above formulas, we can obtain

$$\begin{aligned} &\frac{\partial |y_{q2}(n)|}{\partial w_{mi}(n)} \\ &= \frac{\partial |y_{q2}(n)|}{\partial w^R_{mi}(n)} + j\frac{\partial |y_{q2}(n)|}{\partial w^I_{mi}(n)} \\ &= \frac{1}{|y_{q2}(n)|} [\varphi(c^R_{q2}(n))\varphi'(c^R_{q2}(n))\varphi'(s^R_{q1}(n)) v^R_{ij}(n) x^R(n-m+1) \\ &\quad - \varphi(c^R_{q2}(n))\varphi'(c^R_{q2}(n))\varphi'(s^I_{q1}(n)) v^I_{ij}(n) x^I(n-m+1) \\ &\quad + \varphi(c^I_{q2}(n))\varphi'(c^I_{q2}(n))\varphi'(s^I_{q1}(n)) v^R_{ij}(n) x^I(n-m+1) \\ &\quad + \varphi(c^I_{q2}(n))\varphi'(c^I_{q2}(n))\varphi'(s^R_{q1}(n)) v^I_{ij}(n) x^R(n-m+1) \\ &\quad + j \cdot \frac{1}{|y_{q2}(n)|} \cdot [-\varphi(c^R_{q2}(n))\varphi'(c^R_{q2}(n))\varphi'(s^R_{q1}(n)) \\ &\quad \times v^R_{ij}(n) x^R(n-m+1) \\ &\quad - \varphi(c^R_{q2}(n))\varphi'(c^R_{q2}(n))\varphi'(s^I_{q1}(n)) v^I_{ij}(n) x^R(n-m+1) \\ &\quad + \varphi(c^I_{q2}(n))\varphi'(c^I_{q2}(n))\varphi'(s^I_{q1}(n)) v^R_{ij}(n) x^R(n-m+1) \\ &\quad - \varphi(c^I_{q2}(n))\varphi'(c^I_{q2}(n))\varphi'(s^I_{q1}(n)) v^I_{ij}(n) x^I(n-m+1). \end{aligned} \tag{33}$$

(2). Iteration of the Connection Weight from the Hidden Layer to the Output Layer

Similarly, the iterative formula shall be used to solve the inter-layer connection weight.

$$\frac{\partial |y_{q2}(n)|}{\partial v_{ij}(n)} = \frac{\partial |y_{q2}(n)|}{\partial v^R_{ij}(n)} + j\frac{\partial |y_{q2}(n)|}{\partial v^I_{ij}(n)} \tag{34}$$

In the formula,

$$\frac{\partial |y_{q2}(n)|}{\partial v_{ij}^R(n)} = \frac{\partial \sqrt{y_{q2}(n)y_{q2}^*(n)}}{\partial v_{ij}^R(n)} = \frac{1}{2|y_{q2}(n)|}\frac{\partial [y_{q2}(n)y_{q2}^*(n)]}{\partial v_{ij}^R(n)}$$
$$= \frac{1}{|y_{q2}(n)|}\cdot[\varphi(c_{q2}^R(n))\varphi'(c_{q2}^R(n))b_{q1}^R(n) + \varphi(c_{q2}^I(n))\varphi'(c_{q2}^I(n))b_{q1}^I(n)] \quad (35)$$

Similarly,

$$\frac{\partial |y_{q2}(n)|}{\partial v_{ij}^R(n)} = \frac{1}{|y_{q2}(n)|}\cdot[-\varphi(c_{q2}^R(n))\varphi'(c_{q2}^R(n))b_{q1}^I(n) + \varphi(c_{q2}^I(n))\varphi'(c_{q2}^I(n))b_{q1}^R(n)] \quad (36)$$

Then, we obtain

$$\frac{\partial |y_{q2}(n)|}{\partial v_{ij}(n)} = \frac{\partial |y_{q2}(n)|}{\partial v_{ij}^R(n)} + j\frac{\partial |y_{q2}(n)|}{\partial v_{ij}^I(n)}$$
$$= \frac{1}{|y_{q2}(n)|}\cdot[\varphi(c_{q2}^R(n))\varphi'(c_{q2}^R(n))b_{q1}^R(n) + \varphi(c_{q2}^I(n))\varphi'(c_{q2}^I(n))b_{q1}^I(n)] + \frac{1}{|y_{q2}(n)|}\cdot[-\varphi(c_{q2}^R(n))\varphi'(c_{q2}^R(n))b_{q1}^I(n) + \varphi(c_{q2}^I(n))\varphi'(c_{q2}^I(n))b_{q1}^R(n)] = \frac{1}{|y_{q2}(n)|}$$
$$\cdot[\varphi(c_{q2}^R(n))\varphi'(c_{q2}^R(n)) + j\varphi(c_{q2}^I(n))\varphi'(c_{q2}^I(n))]b_{q1}^*(n). \quad (37)$$

3) CONSTRUCT A DOUBLE-SIGMOID BP NEURAL NETWORK-BASED EXCITATION FUNCTION UNDER INTENSIVE SOCIAL GROUP

Multi-signal blind detection of dense social group communication is a complex problem featured by information-richness and dynamic noise, since different connection structures exist for neurons in different layers [26]–[28]. If different sigmoid functions are added to neurons in different layers, all neurons of the three layers form a new BP neural system-based blind detection system, which is a double-sigmoid system. Multi-threshold sigmoid (EXP) excitation function is used to solve the capacity of processing rich information with only a few neurons, while the improved sigmoid (TANH) excitation function is utilized to solve poor network performance caused by noise error. In this way, challenges brought by social group densification can well be solved, time loss caused by improved anti-noise capacity of a BP neural network can be supplemented, and the convergence efficiency of blind detection network can be effectively improved [29].

In the BP neural network, $\varphi_1(\cdot)$ is the first sigmoid function, while $\varphi_2(\cdot)$ is the second one.

In a traditional continuous neural network, a two-value activation function $\varphi(x)$ is generally selected as the sigmoid function in the form of continuous differentiable single node. Since a neural network is composed of many neurons, it directly determines the network scale, complexity, and robustness [30]. As multi-threshold neurons have multiple excitation states, the application in specific engineering plays a role of uniting neurons of multiple excitatory states. In this way, neuron efficiency is largely improved, and the information processing ability can be accelerated during transmission of circuit signals.

This paper is enlightened by the multiple-valued sigmoid function presented by J.M. Zurada; derivation is based on the two-value sigmoid function $\varphi_1(x) = 2\varphi_s(x) - 1$ (a hyperbola tangent function); and $\varphi_s(x) = (1 + e^{-\lambda x})^{-1}$ is a uni-polarity function. The EXP excitation function is expressed as

$$\varphi_1(x, n) = [\sum_{j=1}^{n}\frac{2\sigma}{1 + e^{-\lambda(x+\theta_j)}}] - n\sigma \quad (38)$$

In the formula, θ_j is the horizontal axis of the center of accumulated meta-functions, n is the total amount of accumulated items, and $n\sigma$ is related with the character set to which signals belong. λ is the attenuation coefficient for function of every accumulated item, and $\lambda > 0$; the value is related with the inflection point amount of an excitation function. 2σ is the phase difference of any two adjacent constellation points of ideal MPSK signals.

A multi-threshold function is characterized by the following three features.

(1). When $x \to +\infty$, $f(x, n\sigma)$ has an absolute maximum $n\sigma$; when $x \to -\infty$, $f(x, n\sigma)$ has an absolute minimum $-n\sigma$, and the function output is bounded.

(2). When $n > 1$, the excitation function has no inverse function with analytical expression.

(3). The function is monotone increasing. Namely, it satisfies $\varphi'(x, n\sigma) > 0$, $[\varphi^{-1}(x, n\sigma)]' > 0$.

The value range of λ and the relation between λ and inflection point are discussed below. The second-order derived function of the function shall firstly be obtained.

$$\varphi_1(\cdot) = [\sum_{j=1}^{n}\frac{2\sigma}{1 + e^{-\lambda(x+\theta_j)}}] - n\sigma = 2\sum_{j=1}^{n}\kappa_s - n\sigma$$
$$\kappa_s(x + \theta_j) = [1 + e^{-\lambda(x+\theta_j)}]^{-1}$$
$$\kappa_s'(x + \theta_j) = \lambda\kappa_s^2(x + \theta_j)\cdot e^{-\lambda(x+\theta_j)}$$
$$\kappa_s''(x + \theta_j) = \lambda^2\kappa_s^3(x + \theta_j)\cdot e^{-\lambda(x+\theta_j)}\cdot[e^{-\lambda(x+\theta_j)} - 1]$$
$$\kappa_s'''(x + \theta_j) = \lambda^2\kappa_s^4(x + \theta_j)\cdot e^{-\lambda(x+\theta_j)}\cdot\{e^{-2\lambda(x+\theta_j)} - 4e^{-\lambda(x+\theta_j)} + 1\} \quad (39)$$
$$\varphi_1'(\cdot) = \{[2\sigma\sum_{j=1}^{n}\kappa_s(x + \theta_j)] - n\sigma\}' = 2\sigma\sum_{j=1}^{n}\kappa_s'(x+\theta_j) = 2\sigma\sum_{j=1}^{n}\lambda\kappa_s^2(x+\theta_j)\cdot e^{-\lambda(x+\theta_j)} \quad (40)$$

$$\varphi_1''(\cdot) = 2\sigma \sum_{j=1}^{n} \kappa_s''(x+\theta_j)$$
$$= 2\sigma \sum_{j=1}^{n} \{\lambda^2 \kappa_s^3(x+\theta_j) \cdot e^{-2\lambda(x+\theta_j)}$$
$$- \lambda^2 \kappa_s^2(x+\theta_j) \cdot e^{-\lambda(x+\theta_j)}\} \quad (41)$$
$$\varphi_1'''(\cdot) = 2\sigma \sum_{j=1}^{n} \kappa_s'''(x+\theta_j)$$
$$= 2\sigma \sum_{j=1}^{n} \lambda^3 \kappa_s^4(x+\theta_j) \cdot e^{-\lambda(x+\theta_j)} \cdot \{e^{-2\lambda(x+\theta_j)}$$
$$- 4e^{-\lambda(x+\theta_j)} + 1\} \quad (42)$$

The relationship between λ value and reflection point is jointly determined by $\varphi''(\cdot) = 0$ and $\varphi'''(\cdot) \neq 0$. However, the second derivative obtained above is a highly non-linear equation. Based on graphical method, $\varphi_1'''(\cdot) \neq 0$ is combined to determine the relationship.

By visualization, for $\pi/4$-QPSK signals, the phase position of the constellation point is $\{\pm\pi/4, \pm 3\pi/4\}$, $\theta_1 = -\pi/2$, $\theta_2 = 0$, $\theta_3 = \pi/2$, $\sigma = \pi/4$, $m = 3$. The expression of the excitation function is expanded as

$$\varphi_1(x, 3\pi/4)$$
$$= \frac{\pi/2}{1+e^{-\lambda(x+\pi/2)}} + \frac{\pi/2}{1+e^{-\lambda x}} + \frac{\pi/2}{1+e^{-\lambda(x-\pi/2)}} - 3\pi/4 \quad (43)$$

Draw the $\gamma = \frac{d^2\varphi_1}{dx^2}(\lambda, x)$ curve surface and equipotential line with λ and x as the independent variables, and draw partial reference plan of $\gamma = 0$. See the following Fig. 2.

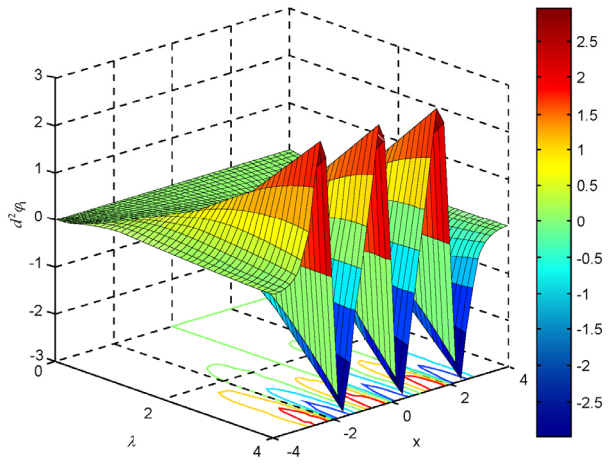

FIGURE 2. $\varphi_1(x, 3\pi/4)$ **Second-order derived function surface and equipotential line plane graph.**

Taking $\pi/4$-QPSK signals and continuous EXP excitation function as the example, continuous EXP excitation functions with different λ value are shown in Fig. 3. When the λ value is large, the image presents sharp-t- flat stepped variation; if the λ value is too small, the image of the excitation function

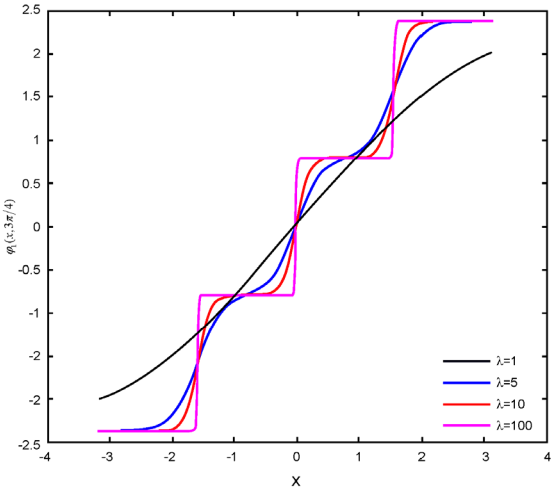

FIGURE 3. $\pi/4$**-QPSK signal, continuous phase multi-thresholds EXP excitation function.**

will not present steps, and the signal screening function of the excitation function is lost.

In a multi-threshold sigmoid excitation function, when x is near the 0 point, $\varphi'(x) > 0$ is located at the maximum. When input values are near 0 point, it will be sensitive, and $\varphi(x)$ will show obvious variation for a tiny change of input value. The absolute value of input value is negatively correlated with noise sensitivity, and is related with poorer self-organizing and self-learning abilities of the neurons. Besides, a BP neural network is a feed-forward network. Deviation of output signals will be extended along with loop iterations, and adversely affects the network performance in the end.

To avoid the above problems, adverse influences caused by a multi-threshold sigmoid excitation function shall be eliminated, and the second sigmoid function $\varphi_2(\cdot)$, is supplemented in the paper as a new improved excitation function. Specifically, the TANH excitation function is expressed as

$$\varphi_2(x) = \begin{cases} \dfrac{\tanh(\xi x_0) + (1 + \tanh(\xi x - x_0))}{1 + \tanh(\xi x_0)} \lambda(x) & (x \geq 0) \\ \dfrac{\frac{1}{2}(1 + \tanh(\xi(x + x_0))}{1 + \tanh(\xi x_0)} \lambda(-x) & (x < 0) \end{cases} \quad (44)$$

In the formula, ξ is the amplification factor of the above function, and represents the gradient of the function: a larger ξ implies a larger angle of the function curve. x_0 is a positive real number, and represents the limit value of neuron input signal. Only when the absolute value of neuron input is larger than x_0 will the angle of the curvilinear figure of the excitation function $\varphi_2(x)$ enlarge. λ is the attenuation coefficient for function of every accumulated item, and $\lambda > 0$.

Via Matlab simulation and the fixed parameter $\xi = 50$, the graph of $\varphi_2(x)$ variation with x_0 is obtained and shown in Fig. 4.

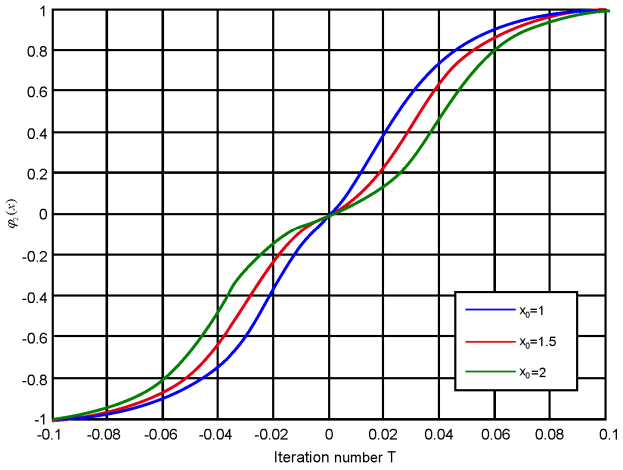

FIGURE 4. Comparison between $\varphi_2(x)$ different parameters and a classic excitation function.

According to the above figure, there is no large difference of state between $\varphi_2(x)$ and the multi-threshold sigmoid excitation function; when x changes, $\varphi_2(x)$ shows same change towards a same direction. Besides, it can be observed from the above figure that the parameter x_0 shows a variation rule like $\varphi_2(x)$, but the sensitivity of network input value is different if it is located at left or right of the original point. Therefore, selecting a proper x_0 value can weaken sensitivity of the excitation function to network input value near the 0 point and then effectively improve the performance of noise resistance. In addition, when the neuron input value is large, it guarantees an improved and accelerated rate of convergence. In conclusion, the TANH excitation function applies to a BP neural network.

4) CONSTRUCT SELF-ADAPTIVE VARIABLE STEP SIZE ON THE BASIS OF PHYSICAL POWER

The BP neural network-based algorithm well overcomes deficiencies of traditional blind detection techniques, and presents outstanding performances. However, simple optimization with gradient descent algorithm is inclined to be trapped by local minimum and sometimes cannot reach a globally optimal solution [31], [32]. To solve this problem, traditional BP neural network model is integrated with the idea of variable step size to create a BP neural network-based variable step size model, wherein close values occurred during self- adaptation process are used to adjust step size and therefore to obtain the feature of self-adaptation. Take the self-adaptive variable step size of the connection weight iteration formula for three layers of a BP neural network as the example. A fixed step size value is changed into dynamic changing variable sizes by learning; by this way, physical power size can be effectively adjusted to solve the conflict between algorithm convergence sate and steady-state deviation and to overcome deficiencies of BP neural network-based traditional detection methods [33]. The model structure is shown as Fig. 5.

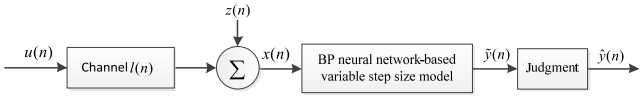

FIGURE 5. Self-adaptation variable Step BP neural network blind equalization algorithm.

In the figure, $u(n)$ is a signaling sequence, $l(n)$ is an unknown channel, $z(n)$ is a noise sequence, and $x(n)$ is received signal sequence. $\tilde{y}(n)$ is the signal restored from the received signal sequence after passing an equalizer, while $\hat{y}(n)$ is the signal obtained after judgment. The equalizer in the figure is modified and superior to a traditional one. It can be applied in abovementioned new BP neural networks.

For the BP neural network-based communication blind signal detection model under QPSK system, we have obtained expressions of the connection weight iteration for the layers. In the expressions, $\eta_1(n)$ and $\eta_2(n)$ are also named variable step sizes. Step size value can be automatically adjusted along with the course of convergence.

$$\eta_1(n) = \eta_2(n) = \beta[\frac{1}{1 - \exp(-\alpha\,|e(n)|^2)} - 0.5] \quad (45)$$

$$e(n) = \hat{y}(n) - \tilde{y}(n) \quad (46)$$

The Adaptive Learning-based Step Size Formula

$$0 \le 1 - \exp(-\alpha\,|e(n)|^2) \le 1$$

$$0 \le \frac{1}{1 - \exp(-\alpha\,|e(n)|^2)} - 0.5 \le \frac{1}{2}$$

$$0 \le \eta_1(n) = \eta_2(n) \le \frac{1}{2}\beta$$

During early algorithm convergence, $|e(n)|$ is relatively large, and so are $\eta_1(n)$ and $\eta_2(n)$ values. When convergence occurs, $|e(n)|$ value decreases continuously, and $1 - \exp(-\alpha\,|e(n)|)$ declines as well; namely, values of step sizes $\eta_1(n)$ and $\eta_2(n)$ decrease as well. It can be known that the variation trend of $|e(n)|$ is close to those of $\eta_1(n)$ and $\eta_2(n)$. Under such variation rule, rate and precision of convergence can both be effectively controlled during such variation course. A large step size value can be obtained from early algorithm and accelerate convergence rate; after convergence, the precision will be improved.

To realize the above plan of algorithm convergence, the step size shall meet the requirements of following formulas.

$$0 \le \eta_1(n) = \eta_2(n) \le \frac{2}{3}tr(R)$$

$$\text{Namely, } \beta \le \frac{4}{3}tr(R) \quad (47)$$

In the formula, R is the autocorrelation matrix of input signal, and $tr(R)$ is the trace of the autocorrelation matrix. Refer to above the formula to determine β value.

In the formula, when the value of β is relatively large, the step sizes $\eta_1(n)$ and $\eta_2(n)$ are relatively large, and the convergence rate of the algorithm is faster than a small

β value case. However, the convergence precision of the algorithm is improved when the β value becomes smaller. It can be found that a faster convergence rate corresponds to a larger β value, while the requirement of a precise convergence course corresponds to a smaller β value.

Generally, selection of α and β values shall refer to algorithm convergence and step size variation trend. Computer simulation is used to select α and β values. On a MATLAB simulation platform, QPSK sending signal is adopted as the input signal; the signal to noise ratio (SNR) is $20dB$; and proper α and β values are selected under two different channel environments. Parameters used in the experiments were selected one by one via simulation, and the selected groups of α and β values effectively indicate how parameters affect algorithm.

Under the channel 1 state, proper α and β values are selected. $\beta = 0.006$ is firstly selected, as it determines algorithm convergence. The β is fixed, while the α varies from $\alpha = 0.0001$ to $\alpha = 0.1$ and $\alpha = 1$ under a dynamic changing course. The α is fixed as $\alpha = 1$, while β varies from $\beta = 0.001$ to $\beta = 0.002$ and $\beta = 0.006$ under a dynamic changing course. Selection of α and β values are shown in Fig. 6 and Fig. 7.

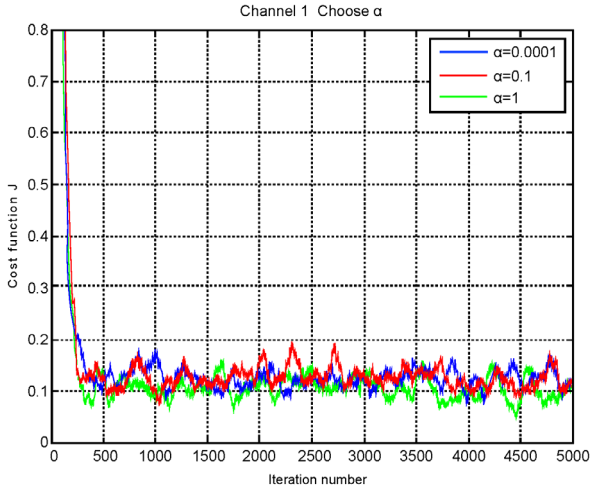

FIGURE 6. Selection of α in the self-adaption variable step BP neural network algorithm under channel 1.

As indicated in Fig. 6, α is less likely to correlate with the algorithm, and the algorithm convergence is better when $\alpha = 1$. It is indicated by Fig. 7 that the model completes algorithm convergence most effectively when $\beta = 0.006$. When $\beta \geq 0.006$, the convergence is unstable. Consequently, the channel 1 is selected as the sending platform, and $\alpha = 1$ and $\beta = 0.006$ are determined under the QPSK modulation system.

Under the channel 1 state, fixed α and β values are selected. Based on the simulation platform, let $\beta = 0.002$ at first to facilitate smooth algorithm convergence. The β is fixed, while the α varies from $\alpha = 1$ to $\alpha = 3$ and $\alpha = 6$ under a dynamic changing course. The α is fixed as $\alpha = 6$, while β

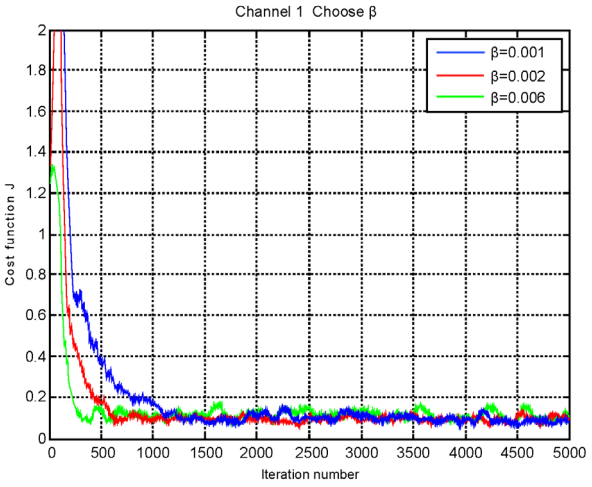

FIGURE 7. Selection of β in the self-adaption variable step BP neural network algorithm under channel 1.

varies from $\beta = 0.0008$ to $\beta = 0.001$ and $\beta = 0.02$ under a dynamic changing course. Selection of α and β values is shown in Fig. 8 and Fig. 9.

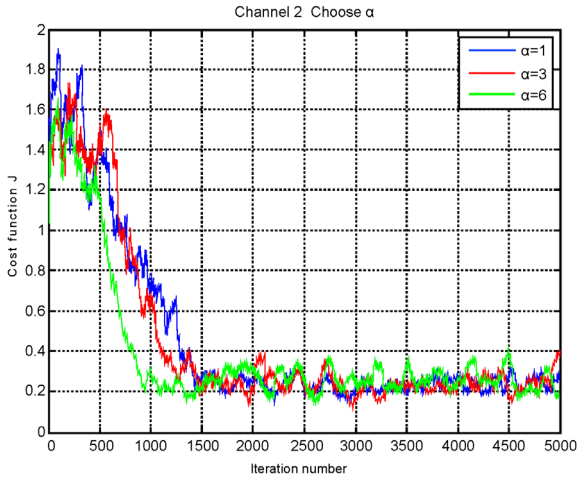

FIGURE 8. Selection of α in the self-adaption variable step BP neural network algorithm under channel 2.

According to Fig. 8 and Fig. 9, the model presents optimal performances when $\alpha = 6$ and $\beta = 0.002$. Consequently, when the channel 1 is the sending platform, and $\alpha = 6$ and $\beta = 0.002$ are selected as the channel 2 condition-based variable step sizes under the QPSK modulation system.

To sum up, steady-state deviation will increase slightly with the acceleration of BP-IVS convergence rate. Since the descent of convergence rate leads to obvious effect, we select the parameters when the convergence rate is high.

A BP neural network model is constructed and then the back-propagation algorithm and BP neural network algorithm are applied and integrated for training blind signal sample

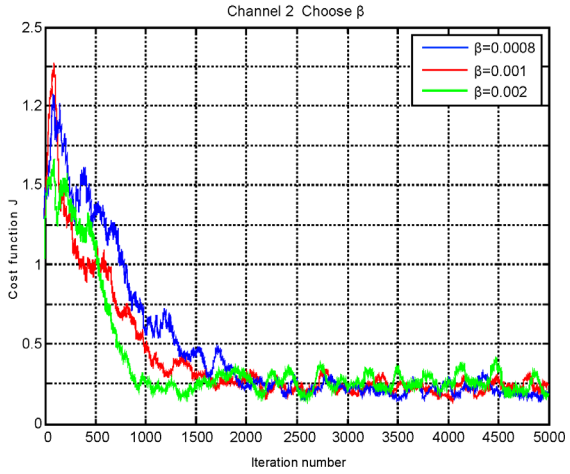

FIGURE 9. Selection of β in the self-adaption variable step BP neural network algorithm under channel 2.

data and adjusting the deviation and network weights, thereby completing the detection and identification of blind signal.

III. EXPERIMENTAL RESULT AND ANALYSIS

Simulation experiments of blind signal detection are conducted to verify the effectiveness of the method presented in this paper, and the platform for the simulation experiments are shown in Fig. 10(a). For the experiments, the hardware environment is Red Hat Enterprise Linux AS 4.0 computer core, and the software environment is Matlab 7. The weight coefficient of the frequency band sampling decision filter is 0.001; the initial value is $\theta_1 = -0.3\pi$; the code element transmission bandwidth for network communication is 200ms; the time interval of network communication outage is 100ms, the disturbance signal to noise ratio (SNR) is -15dB; the transmission signal for network real-time communication is described as $s(n)$ and the frequency is 350Hz; and the sequence bandwidth of information transmitted in network real-time communication by social population is 10KHz $\sim$ 20KHz.

After detecting sound source blind signal, it is further processed. Fig. 10(b) is the computer interface for final processing. The system mainly contains three top modules—a voice frequency load module, a blind signal detection and processing module and a result display module, each of which can be divided into many small functional blocks. Fig. 10(b) can also be called a graphical user interface, as it is the final interface used by researchers to study detection and processing of sound source blind signal and realizes researchers' any conceptions about system functions. It supports not only .fig-files, but also mostly backstage .m-files, which include user input interfaces, output interfaces, relevant widget callback functions required by some computational programming and executing procedures, and completely debugged and separately compiled files. Relevant widget callback functions required by some computational

(a)

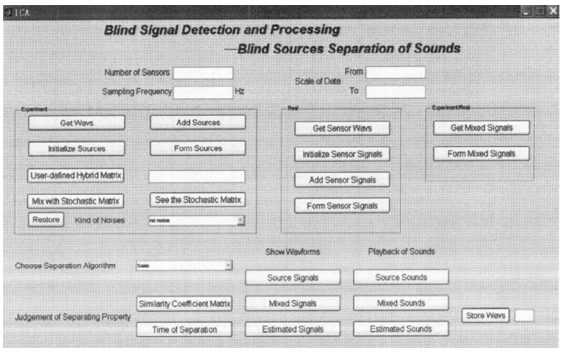

(b)

FIGURE 10. (a) Simulation experiment platform. (b) Blind signal detection and processing system.

programming and executing procedures are saved in m-files; the filenames are same as the names of the user interfaces, and the two present extremely close relevance. A .fig-file is the background operational program executed by an .m-file. During normal operation of the blind signal detection system, all files are processed as a whole.

The operand for time-frequency transformation of signal is directly affected by the amount of sampling point, and the former increases with the latter. As a result, when the amount of sampling point is increased, the effective information from signal detection will also increase, and extracted information features will be more comprehensive and precise with improved information classification precision. However, the method presents certain deficiency—when the amount of sampling point increases to a certain degree, effective information as well as its features will not increase and there will be huge operands, resulting in system crash. To verify the effectiveness of the BP neural network algorithm-based blind signal detection method presented in the paper, the amounts of sampling points in the experiments are set as 256. The dimensionality of extracted signal feature vector is sensitive to the length of Kalser window; the larger the Kalser window length is, the higher the dimensionality of extracted signal feature vector is and the better the signal feature classification effect is. In a similar way, the increase of the Kalser window length will result in a dramatic increase of operand and network load. Therefore, in the paper, the lengths of the

Kalser window are set to 25 and 37, and the obtained nonzero singular value is $(37 + l)/2 = 19$. During the procedure of signal time-frequency transformation, cross term inhibitory effect is more obviously affected by transformation parameters W and N of GRD. Therefore, the two parameters shall be properly set for effective inhibition of the cross term during the time-frequency transformation procedure. To gain favorable effects, in the simulation experiments of the paper, the two parameters are set to WieM/N = 1/5 and rs = 36; the dimensionality of signal feature vector is affected by the amount of BP neural network node, which is set to 19; the amount of BP neural network output node is set as that of the signal classification; the amount of BP neural network intermediate node is closely related with website complexity and computation performance; the higher the amount of intermediate node is, and the better the network performance is, but the network operand and complexity increase as well. So, the relations of the three shall be well weighted. In this paper, the amount of BP neural network intermediate node is 25, and the training error threshold is set to 0.02. An operation keys in "ICA" and carriage return in the MATLAB command line, and the system runs immediately and shows the system final interface as Fig. 10(b).

A. SIMULATION EXPERIMENT 1

Detect a group of original signal sources. The sampling frequency is 11025 Hz; the hybrid matrix is a random matrix; and the data length is N = 15000.

As shown in Fig. 11, the preprocessed signal source is detected for blind signal with the method mentioned in the paper. The BP neural network model goes through 3520 learning times before training stop, and the error between expected output signal and actual output signal is 0.053. It can be viewed from Fig. 11and Fig. 12 that the result based on the method shows one-to-one correspondence for the signal detection peak pattern as well as basically same peak intensities. It can be demonstrated that the method of the

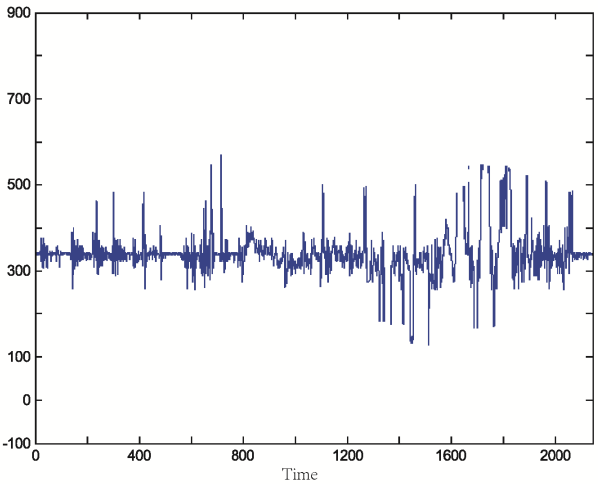

FIGURE 11. Original signal source.

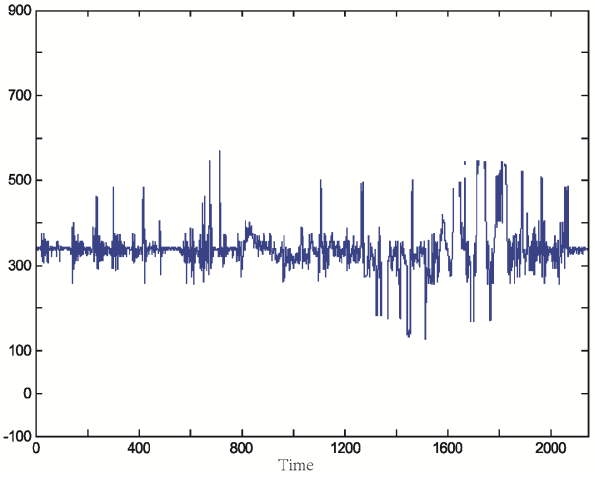

FIGURE 12. Signal detection result.

paper presents relatively high precision for detection signal. Under the precision, the optimal extracted result is shown as Fig. 13, in which the dotted line is the signal extraction result while the solid line is the expected output signal.

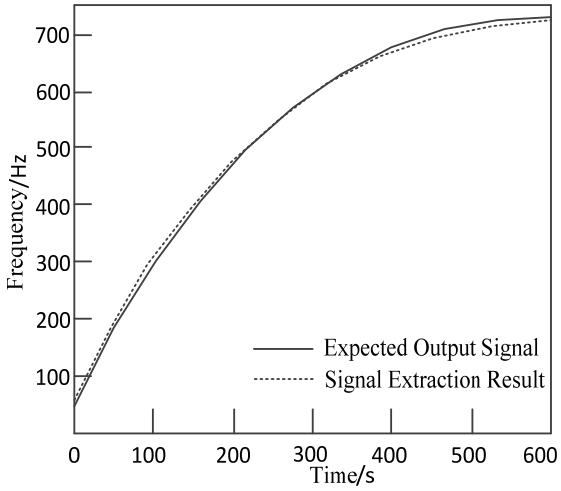

FIGURE 13. Comparison of signal detection extraction.

From Fig. 13, it can be seen that the output signal of the extracted result basically fits the expected signal, and that the basic features of the extracted signal present signal fitting in a point-to-point pattern from the thickest dimension. The final approximation errors of different dimensions are reflected in Tab. 1.

The simulation data shows that the method proposed in the paper is characterized with high precision for blind signal detection fitting and has few errors. For the influencing factor of sensor amount, the paper does not particularly explore the impacts of sensor amount on blind signal detection and processing, because under same conditions the application of more prediction sensors generally leads to more superior global detection or identification performance. For example,

TABLE 1. Learning amount and error approximation for different sizes.

Serial No.	Size	Learning amount	Error result
1	6	796	35.081
2	5	698	22.323
3	4	582	9.289
4	3	592	2.364
5	2	482	0.096
6	1	370	0.053

to identify, detect or separate n signals, the comprehensive effect of applying $n + 1$ sensors will be obviously superior to application of n sensors. However, in actual operation, there is no need to input the variable, because regardless of actual sensor amount, sound signals from different sound sources will be fused and transmitted to different sensors; every sensor receives fused signal, and a computer is used to collect and analyzed the mixed signals. If the signals are stored with MATLAB, the data will be stored in the form of .mat-files, actually a column vector. All column vectors obtained by all sensors compose a mixed signal $x(l)$, a M $*$ N matrix—M indicates data length of every signal (collection point amount) and N suggests the amount of sensor. When a random hybrid matrix is generated subsequently, the matrix row amount is determined by the figure, and the amount of sensor must be input. The ''number of sensors'' is Static Text displaying single-line comment without callback function. The later input box Edit Text has a callback function, which converts character string into bout-precision floating-point format and saves data (the amount of sensor) input by an experimenter.

The method from the Literature [10] and the BP neural network-based blind signal detection method proposed in the paper are respectively used to test 500 groups signal data. The test precision rates and omission rates are shown in Tab. 2. The method from the Literature [10] suggests a detection precision rate of only 73%, while the BP neural network-based blind signal detection proposed in the paper makes the tested signal precision be close to the original values with the repeatedly adjusted and trained sample and realizes a precision rate of 91% for output sample detection, a significantly improved detection precision rate. As to omission rate, the method from the Literature [10] suggests a relatively higher omission rate of 9%, while the BP neural network-based method reduces the omission rate.

TABLE 2. Comparison of simulation detection test indexes.

	Precision Rate	Omission Rate
Method from Literature 10	73%	9%
Method of the Paper	91%	2%

Fig. 14 compares the blind signal detection precision rate and the omission rate between the traditional method and the method proposed in the paper. As suggested by the figure, the BP neural network-based algorithms with cyber-physical-social systems proposed in the paper has a significantly better detection precision rate than that of the method from the Literature [4] (91% vs. 75%). Besides, it is also suggested by Fig. 14 that, compared with the blind signal omission rate associated with the method from the Literature [4] (about 9%), the algorithm proposed in the paper is more excellent for its omission rate (2%, below one quarter of that associated with the Literature [4] method). It is further demonstrated by Fig. 14a and 14b that the method proposed in the paper has a higher detection precision rate, a higher accuracy and a lower omission rate than traditional methods.

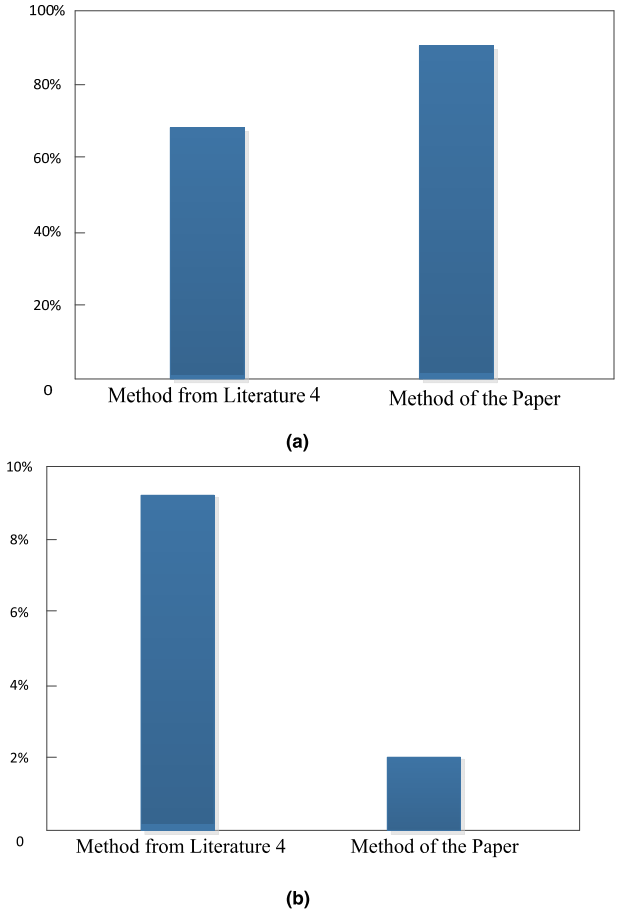

FIGURE 14. (a) Comparison of detection precision rate. (b) Comparison of omission rate.

The experiment compares a traditional method and the method proposed in the paper in terms of a main performance index—error rate, and compares the error rate associated with communication signal detection.

The learning conditions of the two algorithms are shown as Fig.15 and Fig.16. The x-coordinates suggest the amounts of training, while the y-coordinates indicate average error of training. Fig.15 suggests the blind signal detection errors

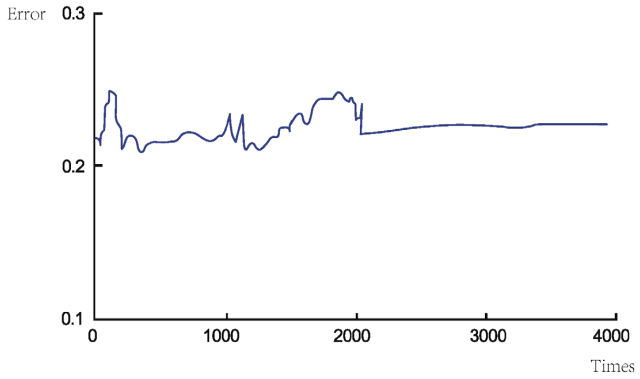

FIGURE 15. Error of the method from literature 9.

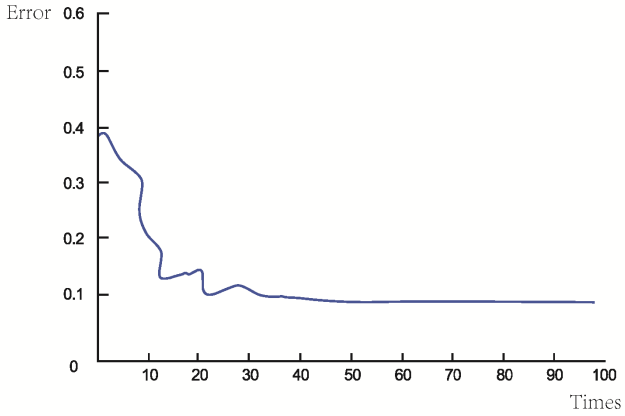

FIGURE 16. Error of the algorithm provided in the paper.

associated with the condition of applying the Literature [9] method, while Fig.16 indicates that associated with the algorithm proposed in the paper. By comparing the two figures, it is clear that the traditional algorithm of the Literature [9] tends to converge after 2000 learning iteration, but the convergence effect is poor, the error rate is unstable, and the value of final error is larger than that of the algorithm proposed in the paper. As for the algorithm proposed in the paper, the curve obviously converge after 30 iterations, there is no great fluctuation, and the final error rate is only 2%.

To sum up, compared with the traditional methods from Literature [10], Literature [4], and Literature [9], the method proposed in the paper is characterized with the advantages of a low omission rate, a low error rate, and high detection precision and accuracy. It can be concluded that the BP neural network-based algorithm with cyber-physical-social systems proposed in the paper is superior to the traditional algorithms in reducing blind signal detection error.

The experiment demonstrates that the BP neural network-based blind signal detection method with cyber-physical-social systems improves detection precision rate while reducing omission rate, and complete blind signal detection in a relatively more effective way. The method proposed in the paper, on the basis of BP neural network algorithm, introduces cyber-physical-social systems, avoids local optimum, and realizes global optimal detection of communication blind signal. It is significantly superior to the traditional methods for its detection performances, which demonstrate high reliability and practical value.

B. SIMULATION EXPERIMENT 2

A group of original signal sources are tested, and the sampling frequency is 11025 Hz. The hybrid matrix is assumed to be

$$A = \begin{bmatrix} 1 & 0.2 & 0.5 \\ 1 & 0.4 & 1 \end{bmatrix}$$

As shown in Fig. 17 and Fig. 18, the algorithm proposed in the paper is used to detect blind signal in the preprocessed signal source.

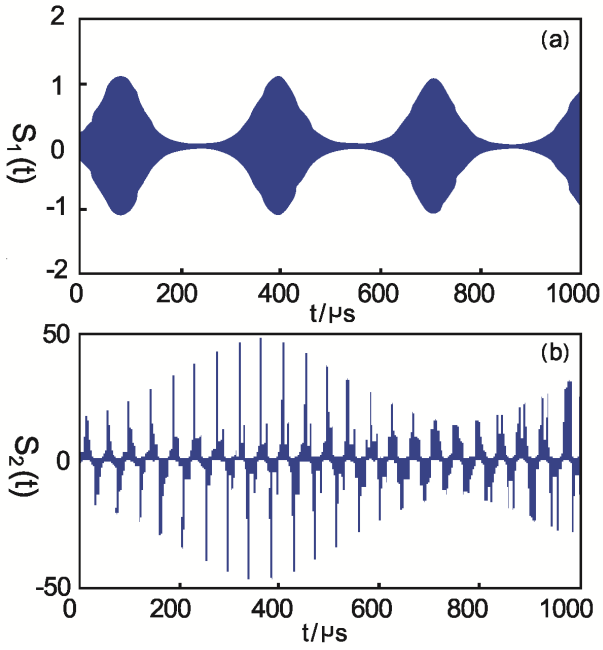

FIGURE 17. (a) The 1st signal of the blind signal source; (b) the 2nd signal of the blind signal source.

According to the simulation data, the result of the blind signal detection using the method proposed in the paper is more precise and less prone to errors; and the results are consistent with those of the Experiment 1.

C. SIMULATION EXPERIMENT 3

In the simulation experiment, the sampling frequency is 11025 Hz; the amount of algorithm iteration is 200; the source signal is sawtooth waves and square waves; and the hybrid matrix with n = 4 and m = 3 is as follow.

$$A = \begin{bmatrix} 1 & 0.7 & 0.6 \\ 0.5 & 1 & 0.8 \\ 0.7 & 0.8 & 1 \\ 0.5 & 0.5 & 0.6 \end{bmatrix}$$

The detection result is shown in Fig. 19.

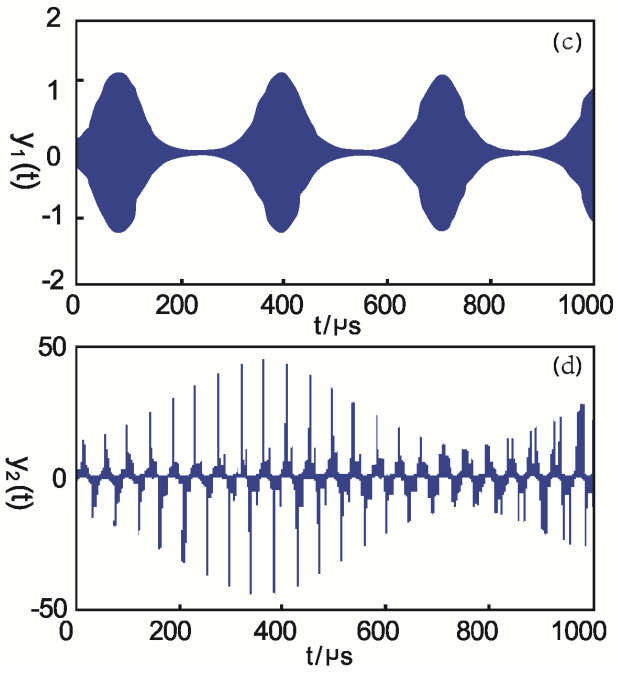

FIGURE 18. (c) The 1st detected signal; (d) the 2nd detected signal.

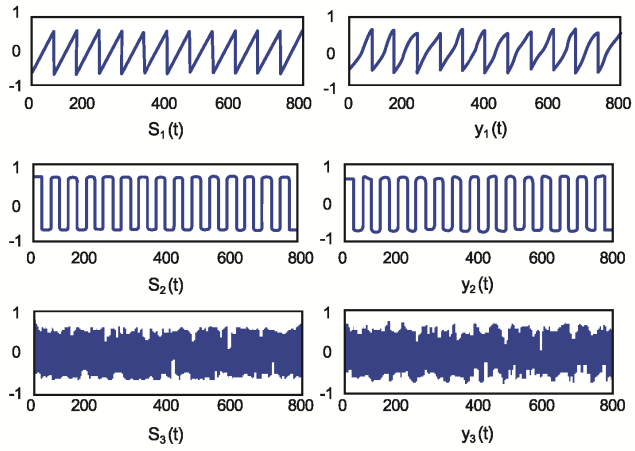

FIGURE 19. Signal detection result of the simulation experiment 3 (The left is the source signal, and the right is the detected signal).

From Fig. 19, it can be seen that the algorithm proposed in the paper effectively detects frequency domain distribution of blind signal, and the detection result is almost identical with the source signal (continuous signal without hopping), verifying that the method effectively detects communication blind signal with a relatively high detection precision and a strong reliability.

D. SIMULATION EXPERIMENT 4

In the simulation experiment, the sampling frequency is 11025 Hz; the source signal is voice signal recorded by the author; the maximal iteration amount is set as 30; and the hybrid matrix is:

$$A = \begin{bmatrix} 0.31 & 0.02 \\ 0.20 & 0.75 \end{bmatrix}$$

The source signal is shown as Fig. 20, while the test result is presented in Fig. 21.

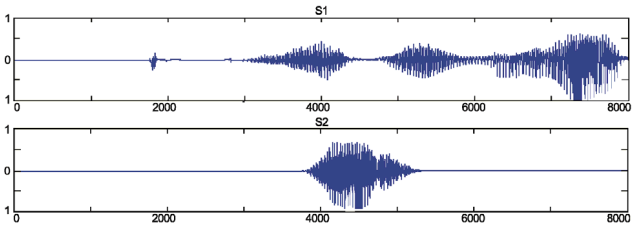

FIGURE 20. Original sources S1 and S2 used in the simulation experiment 4.

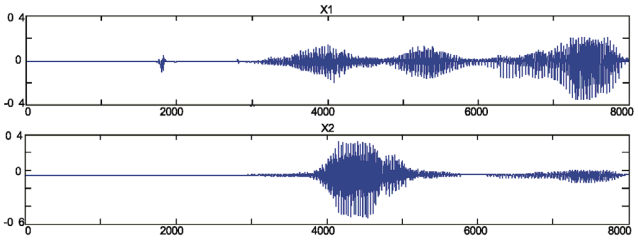

FIGURE 21. Tested signals X1 and X2.

The simulation experiments show that the blind signal detection method proposed in the paper effectively achieves signal detection with a high precision, few errors, a low omission rate and other merits. It overcomes the deficiencies of traditional methods for detection and extraction of blind signal.

IV. CONCLUSION

A BP neural network-based blind signal detection method with cyber-physical-social systems is proposed in the paper. With integrated cyber-physical-social systems, a BP neural network model is constructed for blind signal detection; in a network environment, blind signal obtained from communication devices that are used by social groups, is taken as the data sample and input into the BP neural network model; back-propagation algorithm is used to train and adjust blind signal data derivation and network weight, making output vectors possibly close to expected vectors; the common BP neural network algorithm is integrated with cyber-physical-social systems to avoid problems frequently encountered in a pure BP neural network algorithm, including local minimum and slow algorithm convergence. Experiments are conducted to verify the proposed blind signal detection method, which improves the signal detection precision, reduces the omission rate, and can effectively complete achieve blind signal detection. The detection method is characterized by a high precision (reaching 91%), a small error rate (below 0.1) and

a low omission rate (below 2%), overcomes the deficiencies of traditional methods for detection and extraction of blind signal, and provides a new perspective for precise detection of blind signal. In future work, we will evaluate our proposed model in some realistic scenarios, consider stronger fusion model, and design new solutions under new model.

REFERENCES

[1] H. Urkowitz, "Energy detection of unknown deterministic signals," *Proc. IEEE*, vol. JPROC-55, no. 4, pp. 523–531, Apr. 1967.
[2] B. Qian, Y. Feng, and B. Qian, "An estimation method of direct spread signal pseudo-code rate based on delay-and-multiplication autocorrelation," in *Proc. Int. Symp. Comput. Intell. Des.*, Dec. 2015, pp. 400–403.
[3] L. V. E. Koopmans, "Ionospheric power-spectrum tomography in radio interferometry," *Astrophys. J.*, vol. 718, no. 2, pp. 963–971, 2016.
[4] J. A. A. Qahouq and Z. Xia, "Single-perturbation-cycle online battery impedance spectrum measurement method with closed-loop control of power converter," *IEEE Trans. Ind. Electron.*, vol. 64, no. 9, pp. 7019–7029, Sep. 2017.
[5] G. Liu, M. Ouyang, L. Lu, J. Li, and J. Hua, "A highly accurate predictive-adaptive method for lithium-ion battery remaining discharge energy prediction in electric vehicle applications," *Appl. Energy*, vol. 149, pp. 297–314, Jul. 2015.
[6] J. Jiao, H. Yu, and G. Wang, "A quality-related fault detection approach based on dynamic least squares for process monitoring," *IEEE Trans. Ind. Electron.*, vol. 63, no. 4, pp. 2625–2632, Apr. 2016.
[7] T. C. Mai, M. Egan, T. Q. Duong, and M. Di Renzo, "Event detection in molecular communication networks with anomalous diffusion," *IEEE Commun. Lett.*, vol. 21, no. 6, pp. 1249–1252, Jun. 2017.
[8] M. T. Dabiri and S. M. S. Sadough, "Generalized blind detection of OOK modulation for free-space optical communication," *IEEE Commun. Lett.*, vol. 21, no. 10, pp. 2170–2173, Oct. 2017.
[9] D.-H. Shin and J. Zhang, "Early anomaly detection in an interconnected power grid and communication network: Exploiting interdependent structure of failures," in *Proc. IEEE Global Commun. Conf.*, Dec. 2015, pp. 1–6.
[10] H. Tian, Z. Liu, W. Xi, G. Nie, L. Liu, and H. Jiang, "Beam axis detection and alignment for uniform circular array-based orbital angular momentum wireless communication," *IET Commun.*, vol. 10, no. 1, pp. 44–49, 2016.
[11] K. Kiasaleh, "Delay-and-multiply clock regeneration in APD-based direct-detection optical OOK communication systems," *IEEE Trans. Commun.*, vol. 40, no. 9, pp. 1448–1462, Sep. 1992.
[12] E. Cano and B. Allen, "Multiple-antenna phase-gradient detection for OAM radio communications," *Electron. Lett.*, vol. 51, no. 9, pp. 724–725, 2015.
[13] T. Singh, "Residue number system for fault detection in communication networks," in *Proc. Int. Conf. Med. Imag., m-Health Emerg. Commun. Syst.*, Nov. 2014, pp. 157–161.
[14] A. K. Azad, L. Wang, N. Guo, H. Y. Tam, and C. Lu, "Signal processing using artificial neural network for BOTDA sensor system," *Opt. Express*, vol. 24, no. 6, 6769, 2016.
[15] A. R. Rababaah and D. K. Sharma, "Integration of two different signal processing techniques with artificial neural network for stock market forecasting," *J. Manage. Inf. Decis. Sci.*, vol. 18, no. 2, pp. 63–80, 2015.
[16] L. E. Olcese, G. G. Palancar, and B. M. Toselli, "A method to estimate missing AERONET AOD values based on artificial neural networks," *Atmos. Environ.*, vol. 113, pp. 140–150, Jul. 2015.
[17] E. Valian, S. Mohanna, and S. Tavakoli, "Improved cuckoo search algorithm for feedforward neural network training," *Int. J. Artif. Intell. Appl.*, vol. 2, no. 3, pp. 36–43, 2011.
[18] W. Jia, D. Zhao, T. Shen, S. Ding, Y. Zhao, and C. Hu, "An optimized classification algorithm by BP neural network based on PLS and HCA," *Appl. Intell.*, vol. 43, no. 1, pp. 176–191, 2015.
[19] X. Han, X. Xiong, and F. Duan, "A new method for image segmentation based on BP neural network and gravitational search algorithm enhanced by cat chaotic mapping," *Appl. Intell.*, vol. 43, no. 4, pp. 855–873, 2015.
[20] J. Wang, Y. Wen, Y. Gou, Z. Ye, and H. Chen, "Fractional-order gradient descent learning of BP neural networks with Caputo derivative," *Neural Netw.*, vol. 89, pp. 19–30, May 2017.
[21] M. J. J. P. van Grinsven, B. van Ginneken, C. B. Hoyng, T. Theelen, and C. I. Sánchez, "Fast convolutional neural network training using selective data sampling: Application to hemorrhage detection in color fundus images," *IEEE Trans. Med. Imag.*, vol. 35, no. 5, pp. 1273–1284, May 2016.
[22] Y. Sun, Y. Li, F. Jia, T. Liu, L. Zhang, and Y. Zhang, "A novel feed-forward neural network blind multi-user detection algorithm by augmented Lagrange optimization," in *Proc. IET Conf. Wireless, Mobile Sensor Netw.*, 2009, pp. 8–11.
[23] R. Khordad and H. R. R. Sedehi, "Application of different entropy formalisms in a neural network for novel word learning," *Eur. Phys. J. Plus*, vol. 130, p. 246, Dec. 2015.
[24] Q. Zhang, L. T. Yang, Z. Chen, and P. Li, "A survey on deep learning for big data," *Inf. Fusion*, vol. 42, pp. 146–157, Jul. 2018.
[25] R. Kaur and S. Singh, "An artificial neural network based approach to calculate BER in CDMA for multiuser detection using MEM," in *Proc. Int. Conf. Next Gener. Comput. Technol.*, Oct. 2016, pp. 450–455.
[26] Z. Liu, K. Cheng, H. Li, G. Cao, D. Wu, and Y. Shi, "Exploring the potential relationship between indoor air quality and the concentration of airborne culturable fungi: A combined experimental and neural network modeling study," *Environ. Sci. Pollut. Res.*, vol. 25, no. 4, pp. 3510–3517, 2018.
[27] Q. Zhang, L. T. Yang, Z. Chen, and P. Li, "An improved deep computation model based on canonical polyadic decomposition," *IEEE Trans. Syst., Man, Cybern., Syst.*, to be published. [Online]. Available: http://ieeexplore.ieee.org/document/8015194/
[28] H. Yang, K. Huang, I. M. R. King, and M. R. Lyu, "Maximum margin semi-supervised learning with irrelevant data," *Neural Netw.*, vol. 70, pp. 90–102, Oct. 2015.
[29] M. Goetz *et al.*, "DALSA: Domain adaptation for supervised learning from sparsely annotated MR images," *IEEE Trans. Med. Imag.*, vol. 35, no. 1, pp. 184–196, Jan. 2016.
[30] Q. Zhang and Z. Chen, "A distributed weighted possibilistic c-means algorithm for clustering incomplete big sensor data," *Int. J. Distrib. Sensor Netw.*, vol. 2014, no. 2, pp. 1–8, 2014.
[31] S.-J. Yu, D. Feng, and Y. Zhang, "Blind detection of BPSK signals using hysteretic hopfield neural network," in *Intelligent Automation* (Lecture Notes in Electrical Engineering), vol. 254. Berlin, Germany: Springer-Verlag, 2013, pp. 693–701.
[32] Z. Liu, H. Li, K. Liu, H. Yu, and K. Cheng, "Design of high-performance water-in-glass evacuated tube solar water heaters by a high-throughput screening based on machine learning: A combined modeling and experimental study," *Sol. Energy*, vol. 142, pp. 61–67, Jan. 2017.
[33] Q. Zhang, M. Lin, L. T. Yang, Z. Chen, and P. Li, "Energy-efficient scheduling for real-time systems based on deep Q-learning model," *IEEE Trans. Sustain. Comput.*, to be published. [Online]. Available: http://ieeexplore.ieee.org/document/8016380/

XIN LIU received the B.Sc. degree in management from Xiangtan University in 2006, the master's degree in software engineering from Wuhan University in 2009, and the master's degree in business administration from the Business School, Hunan University of Technology, in 2014. He is currently pursuing the Management Science and Engineering with the Business School, Central South University, mainly engaged in the application of big data and natural language processing in medical fields.

YANJU ZHOU received the bachelor's degree in economics and the M.S. degree in management science from Central South University in 1996 and 2002, respectively, and the Ph.D. degree in management science from Beihang University in 2007. She is currently a Professor and a Doctoral Tutor. She is also an expert in decision science and supply chain management. She has authored or co-authored about 30 articles in academic journals, including *International Journal of Production Economics*, *Knowledge-Based Systems*, *Human and Ecological Risk Assessment: An International Journal*, and *Journal of Intelligent & Fuzzy Systems*.

ZONGRUN WANG received the Ph.D. degree in Management from Central South University, China, in 2004.From 2008 to 2009, he was a Visiting Scholar with California State University, Northridge. He was a Professor and a Doctoral Supervisor with Central South University in 2010, where he has been a Vice Dean with the School of Business since 2014.

He has authored or co-authored some 40 articles in academic journals including *The Australian Economic Review*, *Economic Modeling*, the *Journal of Applied Statistics*, *Physica A: Statistical Mechanics and its Applications*, and the *International Journal of Production*. He has authored three academic works. His research is substantially supported by grants from the National Natural Science Foundation of China. He is a Peer Reviewer for the *Journal of Financial Stability*, the *Journal of Banking and Finance*, and the *International Journal of Production Economics*.

XIAOHONG CHEN was an Academician, a Professor, and a Doctoral Tutor of the Chinese Academy of Engineering. He was the Director and a Chief Professor of National Key Discipline Management Science and Engineering, National Innovation Research Group, Yangtze River Scholar Innovation Team, Ministry of Education and State-Level Teaching Team and National Professional Specialties. He has authored or co-authored over 300 papers in important academic journals at home and abroad, including 33 ESI's top 1% highly-cited papers, 120 SCI and SSCI included papers, over 200 EI, Cssci, and CSCD included papers. As the first person completed the relevant project, won one Second Prize of National Science and Technology Progress, one First Prize and two Second Prizes of Humanities and Social Sciences Outstanding Achievements of Ministry of Education, one First Prize and two Second Prizes of Chinese Science and Technology Award for Universities, Hunan Guangzhao Science and Technology Award, 14 Prizes about the First Prize or Second Prize of Hunan Provincial Scientific and Technological Progress and Provincial Ministerial Level Scientific Awards, one Second Prize of National Teaching Achievements, and one Prize of National Excellent Courses. He was a National Outstanding Youth Fund Winner.